INTERNATIONAL JOURNAL FOR NUMERICAL METHODS IN FLUIDS
Int. J. Numer. Meth. Fluids 2006; **52**:199–211
Published online 10 February 2006 in Wiley InterScience (www.interscience.wiley.com). DOI: 10.1002/fld.1174

Simulation of an impinging jet in a crossflow using a Reynolds stress transport model

Nicholas A. Worth and Zhiyin Yang*,†

Department of Aeronautical and Automotive Engineering, Loughborough University, Loughborough LE11 3TU, U.K.

SUMMARY

An impinging jet in a crossflow is a flow case representative of a jet-lift aircraft operating in ground effect. Accurate modelling of this flow field is essential in predicting the practical flow problems associated with these aircraft; in particular the ingestion of hot gas into the engine intakes, and the importance of the ground vortex contribution towards this. This paper describes a numerical study of this flow using the Reynolds averaged Navier–Stokes (RANS) approach with a Reynolds stress transport model (RSM), validating the current results against experimental data and comparing with other numerical results. A grid-independent solution was determined and the importance of correct inlet geometry modelling demonstrated. Although slight improvements over the eddy-viscosity approach are produced, the RSM model fails to predict the correct ground vortex centre location, and vortex attachment to the impinging jet, demonstrating that the RANS approach used to solve a highly unsteady, time-dependent phenomenon is likely to result in the poor predictions seen. Therefore although the current approach does offer advantages over the k–ε model, it still may only be suitable for gross flow-field approximations, as part of preliminary studies. For more accurate investigation of configuration-dependent effects, further investigation into the LES approach is recommended. Copyright © 2006 John Wiley & Sons, Ltd.

KEY WORDS: impinging jet; jet in a crossflow; VSTOL; Reynolds stress transport model

1. INTRODUCTION

A single impinging jet in a crossflow provides a basis for understanding the dynamics of more complex practical flow fields, and is particularly relevant to the flow field beneath a short takeoff/vertical landing (STOVL) aircraft in ground operation. Knowles and Bray [1] and Cimbala *et al.* [2] describe the nature of the practical flow field and some of the potential problems associated with it. Interaction between the ground plane, and the lift jets of

* Correspondence to: Zhiyin Yang, Department of Aeronautical and Automotive Engineering, Loughborough University, Loughborough LE11 3TU, U.K.
† E-mail: z.yang@lboro.ac.uk

Received 29 July 2005
Revised 6 December 2005
Accepted 7 December 2005

STOVL aircraft can result in a number of operational problems including: lift losses due to enhanced entrainment of the surrounding fluid by the jet flow (suck down); engine thrust losses with potential stall from hot gas ingestion (HGI); and aerodynamic instability from unsteady fountain upwash caused by multiple jet interaction. Of these it is HGI that provides a major design constraint, and has been described as the most important development area for a STOVL aircraft [1]. If re-ingested, the higher temperature fluid will reduce the amount of power produced by the engine. The uneven temperature variations, and turbulent nature of the exhaust gasses also have the potential to cause compressor stall, resulting in a sudden and catastrophic thrust loss.

The three recognized sources of HGI: the near-field or fountain flow, mid-field, and far-field re-circulation of the exhaust gases. The current study will focus on accurate simulation of the far-field or ground vortex contribution, as this is both fundamental to assessing the simulation accuracy, and is a direct source of HGI. A ground vortex is formed upstream of a perpendicular jet in a crossflow, which is impinging on the ground. Without a crossflow the jet fluid would flow radially outwards; when a crossflow is present the upstream jet flow travels against this as near-wall flow before being rolled back onto itself, forming a horseshoe or scarf vortex.

A number of experimental studies have been performed in this area, although the majority of these are based on specific configurations [3–5]. Due to the flow sensitivity to configuration changes, and an incomplete understanding of the flow field interactions, Behrouzi and McGuirk [6] highlight the need for more general research. Studies by Barata *et al.* [7, 8] and Barata and Duão [9] examine the flow field of a single impinging jet in a crossflow using laser Doppler anemometry, highlighting the critical high shear areas around the impingement region, which require particular modelling care. Cimbala *et al.* [2] used high-speed motion pictures and spectral measurements to study the ground vortex, which is observed to be highly unsteady, varying significantly in size. This time-dependent, pulsing nature has obvious implications for HGI, and the ability of any RANS-based method to predict this flow.

Many numerical predictions have also been performed in this area. An entire Harrier aircraft was simulated with the complex multi-jet flow filed [10, 11] but experimental verification of the ground vortex prediction was not available. HGI problem was studied numerically by Page *et al.* [12], Jiang and McGuirk [13]. Barata *et al.* [14] performed a numerical study of single impinging jets in crossflow. Pandya *et al.* [15] carried out unsteady computations of a jet in crossflow with ground effect. The majority of those computations utilizes a turbulence model employing the eddy viscosity approach. Although the gross features of the flow were predicted, the failure to predict the turbulent structure of the impingement zone was attributed to the known shortcomings of the eddy viscosity hypothesis. Ince and Leschziner [16] present a study of both a free jet, and an impinging jet in a crossflow, using two RSM formulations and the k–ε eddy viscosity model. The dependence of the solution upon the turbulence model shows the sensitivity to turbulent anisotropy, and the results highlight the merits of adopting a second moment of closure model, over an eddy viscosity model. Tang *et al.* [17] underline the inability of RANS-based methods in predicting highly unsteady motion such as ground vortex oscillation. The paper states that because knowledge of the time-dependant behaviour is essential to a complete understanding of the flow field, even advanced RSM models still fail to capture all the necessary details. Although a relatively coarse grid was used in the LES study, the simulation still showed some improvement on the RANS k–ε model, particularly in the jet impingement region, where the excellent agreement was seen with the experimental

shear stresses. The LES simulation over predicted the penetration distance however, showing no improvement over the RANS prediction.

LES has been applied to many practical turbulent flow computations due to the development of LES techniques and computing power. However, with the current computing power available LES is still too expensive and cannot be used as routine calculations in industry for practical engineering problems. Hence, there is still a need for further investigation of the RANS-based RSM approach to modelling this flow case, as very few studies using this methodology have been performed [16]. Therefore the focus of this study is to simulate this flow case using a Reynolds stress transport model (RSM), and validate the results against the experimental data of Barata *et al.* [7], demonstrating whether the RANS approach with a RSM can predict such a flow accurately.

2. NUMERICAL PROCEDURE

The fundamental physics will be described through the conservation laws for mass and momentum, with additional terms for modelling the turbulence. These equations are fairly standard and will be presented briefly here. The current numerical study matches the experiments [7] with water as the working fluid and hence the flow is incompressible. The time-averaged governing equations in the steady form are as follows:

$$\frac{\partial U_i}{\partial x_i} = 0 \tag{1}$$

$$\frac{\partial U_i}{\partial t} + \frac{\partial (U_i U_j)}{\partial x_j} = -\frac{1}{\rho}\frac{\partial P}{\partial x_i} + \frac{\partial}{\partial x_j}\left[\nu \frac{\partial U_i}{\partial x_j}\right] - \frac{\partial (u_i u_j)}{\partial x_j} \tag{2}$$

By using manipulated forms of the Navier–Stokes equations, transport equations can be derived to govern the Reynolds stresses.

$$\begin{aligned}\frac{\partial(\rho\overline{u_i u_j})}{\partial t} + \frac{\partial(\rho U_k \overline{u_i u_j})}{\partial x_k} = &-\frac{\partial[\rho\overline{u_i u_j u_k}] + \overline{p(\delta_{jk}u_i + \delta_{ik}u_j)}}{\partial x_k} \\ &+ \frac{\partial}{\partial x_k}\left[\mu\frac{\partial(\overline{u_i u_j})}{\partial x_k}\right] - \rho\left[\overline{u_i u_k}\frac{\partial U_j}{\partial x_k} + \overline{u_j u_k}\frac{\partial U_i}{\partial x_k}\right] + \overline{p\left[\frac{\partial u_i}{\partial x_k} + \frac{\partial u_j}{\partial x_k}\right]} \\ &- 2\mu\overline{\frac{\partial u_i}{\partial x_k}\frac{\partial u_j}{\partial x_k}} - 2\rho\Omega_k(\overline{u_j u_m}\varepsilon_{ikm} + \overline{u_i u_m}\varepsilon_{jkm})\end{aligned} \tag{3}$$

Several terms in this exact transport equation need to be modelled. The turbulent diffusive transport term can be modelled using the generalized gradient diffusion model of Daly and Harlow [18]. However due to numerical instabilities generated by this model, it has been simplified:

$$D_{T,ij} = \frac{\partial}{\partial x_k}\left[\frac{\mu_t}{\sigma_k}\frac{\partial(u_i u_j)}{\partial x_k}\right] \tag{4}$$

Lien and Leschziner [19] derived a value of $\sigma_k = 0.82$ by applying the generalized gradient-diffusion model, to the case of a planar homogeneous shear flow. Gibson and Launder [20] proposed the following pressure–strain model:

$$\phi_{ij} = \phi_{ij,1} + \phi_{ij,2} + \phi_{ij,w} \tag{5}$$

$$\phi_{ij,1} = -C_1\rho\frac{\varepsilon}{k}\left[\overline{u_i u_j} - \frac{2}{3}\delta_{ij}k\right], \quad \phi_{ij,2} = -C_2\left[(P_{ij} + F_{ij} + C_{ij}) - \frac{2}{3}\delta_{ij}(P - C)\right]$$

$$\phi_{ij,w} = C_1'\left[\overline{u_k u_m}n_k n_m\delta_{ij} - \frac{3}{2}\overline{u_k u_i}n_k n_j - \frac{3}{2}\overline{u_k u_j}n_k n_i\right]\frac{0.4k^{3/2}}{\varepsilon d}$$

$$= C_2'\left[\Phi_{km,2}n_k n_m\delta_{ij} - \frac{3}{2}\Phi_{ik,2}n_k n_j - \frac{3}{2}\Phi_{jk,2}n_k n_i\right]\frac{0.4k^{3/2}}{\varepsilon d}$$

where $C_1 = 1.8$, $C_2 = 0.60$, $C_1' = 0.5$, $C_2' = 0.3$, d is normal distance to the wall.

The modelled transport equation for the dissipation rate is

$$\frac{\partial(\rho\varepsilon)}{\partial t} + \frac{\partial(\rho\varepsilon U_i)}{\partial x_i} = \frac{\partial}{\partial x_i}\left[\left(\mu + \frac{\mu_t}{\sigma_\varepsilon}\right)\frac{\partial\varepsilon}{\partial x_j}\right] + \frac{1}{2}C_{\varepsilon 1}P_{ii}\frac{\varepsilon}{k} - C_{\varepsilon 2}\rho\frac{\varepsilon^2}{k} \tag{6}$$

where $\sigma_\varepsilon = 1.0$, $C_{\varepsilon 1} = 1.44$, $C_{\varepsilon 2} = 1.92$.

The computer code used is Fluent 6.1 [21] and the second-order upwind scheme is employed. The standard wall functions based on the proposal of Launder and Spalding [22] are applied.

A $1.5 \times 0.1 \times 0.5$ m (streamwise $\times$ wall-normal $\times$ spanwise) domain was created and meshed using Gambit, matching the experimental water flow tunnel dimensions [7]. Both square and circular jet inlet geometry was tested, and contrary to other numerical studies [17] the solution was found to be sensitive to this inlet geometry. Therefore in order to match the experimental set-up, a 0.02 m (D) circular inlet face was created 0.4 m downstream of the crossflow inlet face, on the upper wall and in a central location. Grid refinement was applied around the high shear impingement zone, and close to the impinging wall.

Grid sensitivity studies were carried out, allowing a grid-independent solution to be established. The coarse mesh consists of $110 \times 35 \times 70$ cells along the streamwise, wall-normal and spanwise directions, a total of 269 500 cells. The medium mesh consists of $135 \times 40 \times 105$, a total of 567 000 cells. The fine mesh consists of $135 \times 80 \times 105$ cells, a total of 1 134 000 cells and the very fine mesh consists of $160 \times 100 \times 120$, a total of 1 920 000 cells. The results by the fine and the very mesh agree very closely with a maximum difference in turbulence stresses less than 5%. Therefore all other studies such as inlet boundary condition sensitivities study were performed using the fine mesh and all results presented here are also obtained using the fine mesh.

The Reynolds number is the same as in the experiment (60 000) based on jet inlet conditions. Uniform jet and crossflow velocities of 3 and 0.1 m/s, respectively, were applied at the inlet boundaries. For uniform inlet conditions, values of k, ε, and normal stresses were derived from the measured turbulent intensities and the estimated length scales while the shear stresses were assumed to be zero. Inlet boundary condition sensitivity studies were carried out using profiled inlet conditions. The inlet profiles were created using a number of assumptions. The

crossflow was assumed to be largely uniform, with thin boundary layers present on upper and lower walls as described by Behrouzi and McGuirk [6]. The jet inlet was also approximated using the jet exit detailed in Reference [6]. The results downstream by both the uniform and profiled inlet conditions did not show much discrepancy and the results presented here are obtained by the uniform inlet boundary conditions. A zero gradient outflow boundary was applied downstream on the outlet face.

3. RESULTS AND ANALYSIS

Figure 1 shows a streamline plot of the ground vortex and compares the current predicted gross features of the ground vortex with those of the experimental study [7] and other numerical results by k–ε model [14] and by LES [17].

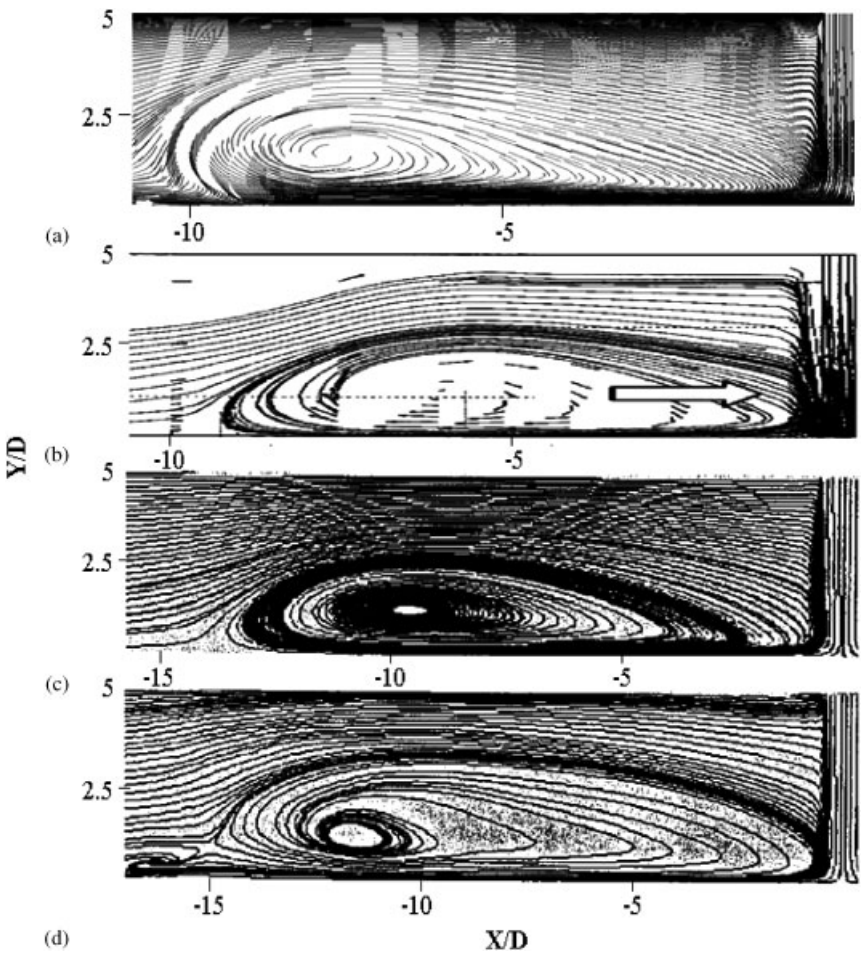

Figure 1. Ground vortex comparison in the central plane of the spanwise direction ($Z/D = 12.5$): (a) RSM; (b) experiments; (c) k–ε; and (d) LES.

The ground vortex length predictions vary considerably between the numerical results. The ground vortex length is defined here as the distance between tip of the ground vortex to centre of the jet. The figure shows that the experimental one is about 9.3D and predictions by the RSM is about 10.5D, by the k–ε model is about 13.2D and by LES is about 14.8D. The over prediction by the LES solution may be attributed to the lack of grid resolutions, and use of square inlet geometry. The RSM length prediction is the closest to the experimental results, about 1.2D (approximately 13%) from the experimental results. The k–ε model is known to suppress separation after impingement, which may contribute to its over prediction of the ground vortex length.

All the numerical results give reasonable vortex height (defined as the maximum height of the ground vortex) predictions. The experimental result is about 2.9D and the prediction by the RSM is about 3.3D, by the k–ε model is about 2.5D and by LES is about 3.4D differing by approximately the same margin of 0.2D or 7%. The RSM and LES solutions over predict this height, and the k–ε under predicts it. The predicted vortex centre height varies little between the models, however the lateral position of the vortex centre varies considerably. It is most clearly illustrated by the relative position of the centre from the ground vortex leading edge. The experimental centre is around 42%, and all of the numerical solutions under predict this; the k–ε model is closest at 33%, but the RSM and LES are both quite short with values of 21 and 23%, respectively. This centre misalignment causes the vortex shape to differ from the experimental shape. The numerical results, and in particular the RSM solution show a greater degree of asymmetry, with fluid concentrated towards the leading edge; the higher degree of taper gives a narrow trailing edge. The vortex centre position will also effect the flow deflection around the ground vortex, and may cause the unexpected reverse fluid flow after separation at the leading edge.

An interesting difference occurs in the ground vortex predictions presented by Ince and Leschziner [16] when the RSM model dissipation rate is sensitized to anisotropy. Although the paper concludes that differences between the variants are not conclusive, a dramatic rearward shift in the vortex centre is shown for the sensitized model. It may therefore be conjectured that poor dissipation rate modelling may cause the current inadequate centre prediction.

Another important factor in correct ground vortex simulation is location. The experimental result (Figure 1(b)) clearly shows the ground vortex trailing edge is attached to the impinging jet, strongly influencing the flow field. The LES result shows this attachment, however both the k–ε and the RSM models fail to predict this, instead positioning the vortex trailing edge further upstream by 1.5D and 0.25D, respectively. Although these predictions are close, this separation will have profound implications for the flow field.

Figures 2(a)–(c) show the predicted mean horizontal velocity profiles at three locations upstream of the impingement location, with excellent agreement between the experimental and numerical results. These figures highlight the accurate wall jet entrainment modelling through peak velocity reduction, from $U/V_j = -0.8$ to -0.26, and substantial profile thickening. The wall jet magnitude will directly influence the ground vortex length, and therefore confidence is gained by the model's ability to correctly capture this critical flow aspect. The other numerical results are only available at the station close to the impingement location (Figure 2(c)) and they all agree with each other very well with a lightly lower peak value predicted by the k–ε model.

Downstream of impingement (Figures 2(d) and (e)) reasonable general agreement between numerical and experimental profiles is seen. Further from the jet however (Figure 2(e)) the

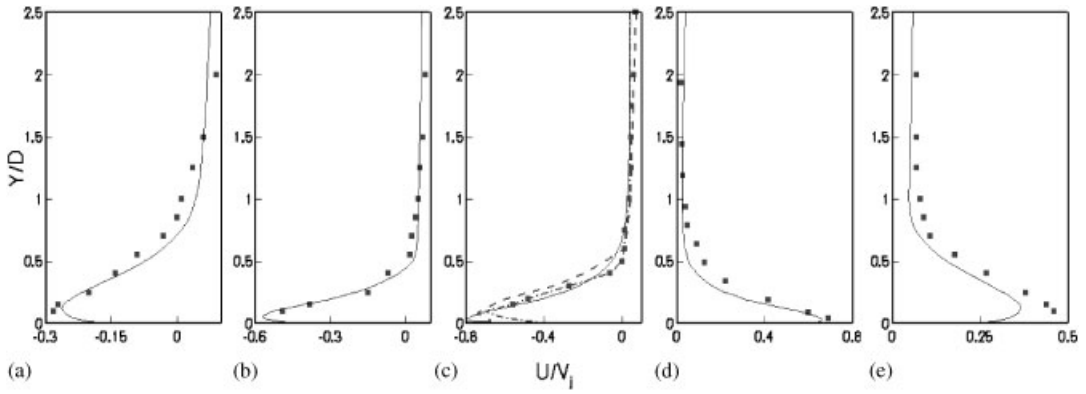

Figure 2. Mean axial velocity profiles at five streamwise locations. Solid line, RSM; symbols, experimental data; dashed line, k–ε; dash–dotted line, LES: (a) $(X - X_j)/D = -4$; (b) $(X - X_j)/D = -1.5$; (c) $(X - X_j)/D = 0.75$; (d) $(X - X_j)/D = 1.5$; and (e) $(X - X_j)/D = 4$.

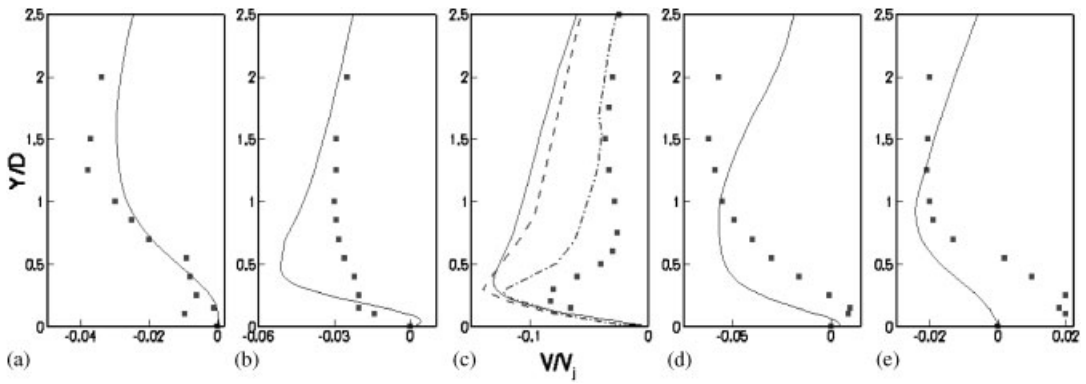

Figure 3. Mean vertical velocity profiles at five streamwise locations. Solid line, RSM; symbols, experimental data; dashed line, k–ε; dash–dotted line, LES: (a) $(X - X_j)/D = -4$; (b) $(X - X_j)/D = -1.5$; (c) $(X - X_j)/D = 0.75$; (d) $(X - X_j)/D = 1.5$; and (e) $(X - X_j)/D = 4$.

numerical solution under predicts the profile significantly. This over-swift wall jet attenuation may be caused by poor transport modelling in the region following jet impingement, and ground vortex location. Ground vortex attachment to the impinging jet causes a large flow obstruction, ensuring more low momentum wake fluid, which can be drawn into the downstream wall jet [9]. The reduced blockage resulting from the forward location, and slender trailing edge of the RSM ground vortex in the present study, may result in higher momentum fluid in and around the lower half of the impinging jet wake region, which may not be drawn into the wall jets as readily. Finally inaccuracies in the velocity predictions may be caused by the sparser grid resolution used downstream of the impingement location.

Figure 3(a)–(c) compare the predicted mean vertical velocity profiles upstream of impingement with the experimental data and other numerical results (Figure 3(c)). Closer

to impingement ($(X - X_j)/D = -0.75$) the velocity is significantly over predicted by both the RSM and k–ε models while the LES results show a much better agreement with the experimental data (Figure 3(c)). This may be mainly caused by the incorrect ground vortex trailing edge location predicted by the RSM and k–ε model as discussed before. The small negative regions in the experimental profiles in the near-wall region indicate the flow attachment to the wall until separation further upstream. This detail is important as this behaviour will affect the skin friction, and heat transfer to the ground plate in the practical application. The very small positive region near to the wall (Figure 3(b)) may indicate flow lifting for a small region above the ground plate, although the flow clearly does not separate until much further upstream.

Flow downstream of impingement (Figures 3(d) and (e)) is greatly influenced by the upstream flow obstructions. Flow blockages produce 'lifting' of the downstream wall jet, which grows at an increased rate due to absence of fluid in the wake region, as shown by the positive mean vertical velocity near the wall. The current predicted results by the RSM model show significant divergence from the experimental results, failing to predict the positive vertical velocity next to the wall (Figure 3(e)). The detached ground vortex creates less flow obstruction, giving rise to more fluid in the wake of the impinging jet and reducing downstream wall jet lifting. Barata and Durão [9] show that wall jet lifting is not seen for a fully detached vortex regime associated with higher velocity ratio flow, which supports this explanation.

Figure 4 compares the predicted normal stress profiles with the experimental data and the LES results at two upstream locations. Although both numerical profiles are similar, the RSM model predicts more accurate near-wall behaviour for the axial stress profiles. The LES inaccuracies, especially the poor near-wall modelling is most likely caused by inadequate grid resolution in the near-wall region. Poor transport and diffusion modelling may cause the over predictions seen by the RSM model. Additionally, the inadequate redistribution of Reynolds stresses may be caused by poor pressure–strain modelling, after break down of the

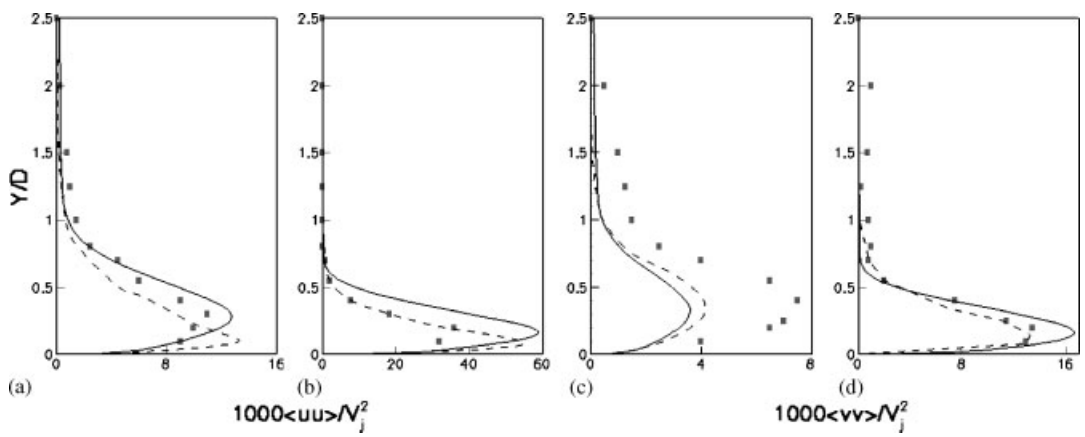

Figure 4. Mean axial and vertical normal stresses at two streamwise locations. Solid line, RSM; symbols, experimental data; dashed line, LES: (a) $(X - X_j)/D = -4$; (b) $(X - X_j)/D = -1.5$; (c) $(X - X_j)/D = -4$; and (d) $(X - X_j)/D = -1.5$.

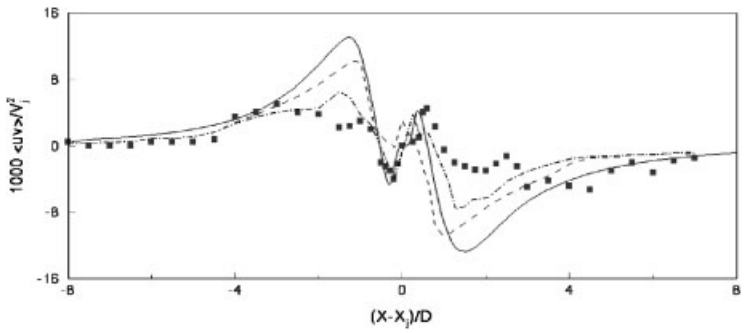

Figure 5. Mean shear stress distribution near the impinging wall ($Y/D = 0.3$). Solid line, RSM; symbols, experimental data; dashed line, k–ε; dash–dotted line, LES.

assumptions in the high curvature impingement zone [7]. Despite these inaccuracies the RSM model shows sensitivity to the turbulent anisotropy. Since linear eddy-viscosity models are known to predict turbulent anisotropy poorly, the solution will benefit from the RSM model.

Figure 5 shows shear stress near the impingement wall. The over prediction of the peak values by the RSM model is immediately apparent. The failure of the RSM model to improve on the k–ε model for these peaks is surprising; due to the reported ability of the RSM model to predict streamline curvature. However, in the inner-impingement region the RSM model replicates the stress distribution shape and magnitude much better than the k–ε model. The slight forward shift of the RSM stresses is expected to stem from poor prediction of the impinging jet deflection. Within this region the RSM model shows clear improvement over the k–ε prediction, which at times even predicts the wrong sign of shear stress. This relates to a breakdown of the eddy-viscosity hypothesis in the impingement region. The LES results show a much better overall agreement with the experimental data. The similarity between the RSM and k–ε model in this region provides evidence that the same problems affect both models. Although poor modelling of the high curvature region may affect the predictions, the highly unsteady nature of the flow field is a more likely source of the numerical scheme failure.

It is worth mentioning that RSM models do not always show an indisputable superiority over two-equation turbulence models. One of the reason is that many more terms need to be modelled. The pressure–strain term, responsible for redistributing the turbulent stress among components to make turbulence more isotropic, is very difficult to model. When computing wall bounded flows some extra terms are usually needed to account for the so-called 'wall-reflection' or 'wall-echo' effects. The RSM results presented above have been obtained using the Gibson and Launder [20] pressure–strain model including the 'wall-echo' term as shown in Equation (5). Two other pressure–strain models have also been tested in the current study in order to see how big effects the pressure–strain term on the flow fields predictions. Those are the linear pressure–strain model with low-Reynolds number modifications proposed by Launder and Shima [23] and the quadratic pressure–strain model by Speziale *et al.* [24]. The quadratic pressure–strain model does not require a correction to account for the wall-reflection effect. The results obtained with the pressure–strain model with low-Reynolds number modification are more or less the same with hardly any recognizable difference in mean velocity profiles

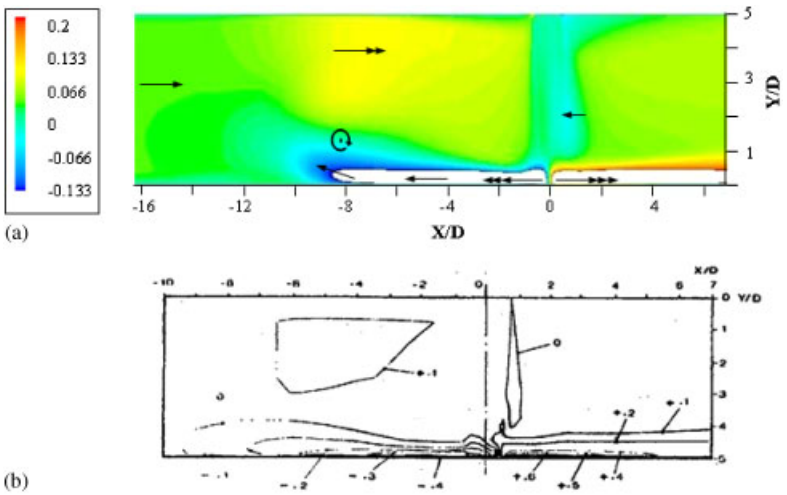

Figure 6. Contours of the mean axial velocity (U/V_j): (a) RSM; and (b) experimental.

and 2% in turbulent stresses. However, slight improvements have been achieved when using the quadratic pressure–strain model with no extra wall-echo term although the predicted flow features are still very similar. The mean velocity profiles are more or less the same but turbulent quantities agree slightly better with the experimental data. The maximum difference in turbulent stresses between the results by Gibson and Launder pressure–strain model [20] and the quadratic pressure–strain model [24] is about 6%. Basara *et al.* [25] reached similar conclusions in the study of an axisymmetric jet impinging on a plane.

Figure 6 shows contours of the mean axial velocity, illustrating wall jet deceleration, a secondary re-circulation region in the impinging jet wake, and the accelerated flow region over the ground vortex. Although the RSM model does predict the gross features of the flow and a reasonably good comparison with the experimental results has been obtained. However, a number of discrepancies are present, which will affect the ability of the model to accurately simulate the practical application. Lifting of the wall jets from the ground plate at the separation position is seen, which is associated with poor ground vortex leading edge prediction, highlighted in the streamline comparison. The numerical model also predicts approximately equal peak magnitudes for upstream and downstream wall jets ($U/V_j = 0.8$), over estimating the experimental peaks, and showing greater symmetry. This may be caused by under prediction of the impinging jet curvature. The forward ground vortex centre position is thought to reduce the flow magnitude over the ground vortex by eliminating vorticity-induced acceleration. This will result in under prediction of the low-pressure region, and the associated lift-losses for the jet-lift aircraft in the practical application. The accelerated flow passing over the ground vortex will also affect the deflection of impinging jet, as it impinges upon this directly.

Figure 7 shows the mean vertical velocity contours, highlighting the entrainment with the impinging jet. The plot also shows the ground vortex centre, between upstream opposite positive and negative velocity regions. The experimental results show that the impinging jet

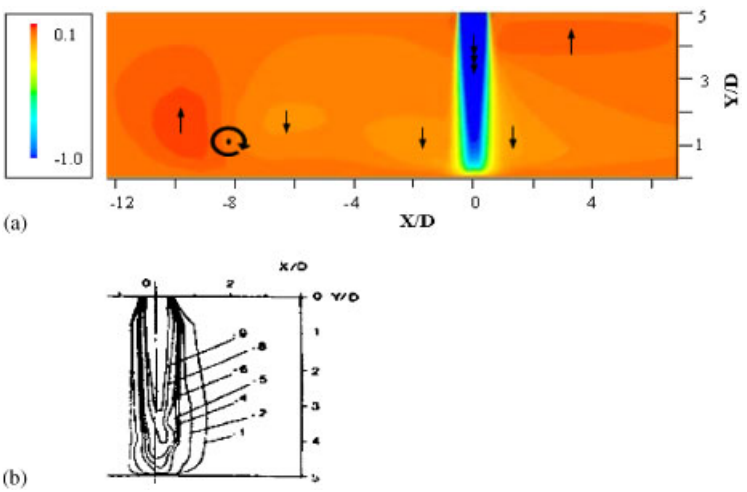

Figure 7. Contours of the mean vertical velocity (V/V_j): (a) RSM; and (b) experimental.

is not symmetric due to the crossflow. However, the current predictions exhibit a higher degree of symmetry, with the impinging jet only deflecting by approximately $X/D = 0.05$, a quarter of the experimental deflection. This puts the results more inline with a fully detached ground vortex regime normally associated with higher velocity ratio flow. The jet deflection is caused by the crossflow, and under prediction of the accelerated region over the ground vortex may contribute to the poor prediction of this.

An unsteady RANS investigation was also conducted, and although some pulsing and velocity fluctuations are observed, indicating possible vortex shedding which could be captured by unsteady RNAS. However, the mean results did not show any improvements over the steady RNAS results, and especially did not capture 'some important unsteady features' due to turbulence which were evident in the LES results [17]. This clearly demonstrates that some important turbulent unsteady flow features can only be captured by LES or DNS.

4. CONCLUSIONS

The current study aimed to validate and assess the performance of the RSM turbulence model for a single impinging jet in a crossflow. The flow case is representative of the more complex practical flow field beneath a jet-lift aircraft operating in the ground environment. To this end the results of the current investigation were compared with the experimental results of Barata *et al.* [7], and other numerical results by k–ε model and LES [14, 17].

During model set-up it was noted that the ground vortex separation length and normal stress distributions showed significantly sensitivity to the jet inlet geometry, and therefore circular geometry was employed.

The RSM model shows a number of improvements over the k–ε model, such as the ground vortex length, ability to predict flow field anisotropy, and the inner-impingement zone shear

stress predictions. However the model fails to accurately predict the ground vortex shape and location. The vortex centre is too far forward, which may account for the poor leading edge shape, and under predicted velocity over the ground vortex. The RSM model also fails to predict the attachment of the ground vortex to the impinging jet, which may result in poor prediction of the upstream vertical velocity profiles, and downstream wall jet lifting.

The ground vortex contributes the far-field element to HGI [1], and although the RSM model describes the average amount of re-circulating fluid reasonably well, the poor shape and location predictions will result in incorrect distribution of this fluid. More fundamentally however, the truly unsteady turbulent flow features cannot be captured by even a unsteady RANS approach.

This flow is a relatively simple building block of the more complex practical flow field, and therefore accurate prediction of the more complex flow field beneath a jet-lift aircraft may be beyond this RANS method. Although the RSM model shows improvement over eddy-viscosity-based models, the accuracy of its predictions are still inadequate in providing more than a gross approximation to the flow field, and the true unsteady nature of the flow is not represented. Therefore the current investigation and other similar studies [14, 16, 17] suggest RANS-based methods may only be suitable for preliminary design work, with more detailed configuration design and HGI prediction having to rely on experimental investigation, and possibly by LES in the near future with increasing computing power and more refined LES techniques.

ACKNOWLEDGEMENTS

The authors gratefully acknowledge the useful suggestions and discussions with Prof. J. J. McGuirk.

REFERENCES

1. Knowles K, Bray D. Recent research into the aerodynamics of ASTOVL aircraft in ground environment. *Proceedings of the Institute of Mechanical Engineers*, Part G. *Journal of Aerospace Engineering* 1991; **205**: 123–131.
2. Cimbala JM, Billet ML, Gaublomme DP, Oeflein JC. Experiments on the unsteadiness associated with a ground vortex. *AIAA Journal of Aircraft* 1991; **28**:261–267.
3. Andreopoulous J, Rodi W. Experimental investigation of jets in crossflow. *Journal of Fluid Mechanics* 1984; **138**:93–127.
4. Kelso R, Lim T, Perry A. An experimental study of round jets in crossflow. *Journal of Fluid Mechanics* 1996; **306**:111–144.
5. Smith S, Mungal M. Mixing, structure and scaling of the jet in crossflow. *Journal of Fluid Mechanics* 1998; **357**:83–122.
6. Behrouzi P, McGuirk JJ. Experimental data for CFD validation of the intake ingestion process in STOVL aircraft. *Journal of Flow Turbulence and Combustion* 2000; **64**:233–251.
7. Barata JMM, Durão DFG, Heitor MV, McGuirk JJ. The turbulence characteristics of a single impinging jet through a crossflow. *Experimental Thermal and Fluid Science* 1992; **5**:487–498.
8. Barata JMM, Durão DFG, Heitor MV, McGuirk JJ. Impingement of single and twin turbulent jets through a crossflow. *AIAA Journal* 1991; **29**:595–602.
9. Barata JMM, Durão DFG. Laser Doppler measurements of impinging jet flows through a crossflow. *Experiments in Fluids* 2004; **36**:665–674.
10. Smith MH, Chawla K, Van Dalsem WR. Numerical simulation of a complete STOVL aircraft in ground effect. *AIAA Paper No. 91-3293*.
11. Chaderjian NM, Pandya SA, Ahmad J, Murman SM. Parametric time-dependent Navier–Stokes computations for a YAV-8B Harrier in ground effect. *AIAA Paper No. 2002-0950*.
12. Page GJ, Jiang D, McGuirk JJ, Harper C. Application of computational fluid dynamics to hot gas ingestion modelling. *International Power Lift Conference*, London, U.K., 1998; 23.1–23.11.

13. Jiang D, McGuirk JJ. A numerical study of intake ingestion revelant to short take-off and vertical landing aircraft. *Proceedings of International Conference on Applied CFD*, Beijing, PR China, 2000; 1–8.
14. Barata JMM, Durão DFG, McGuirk JJ. Numerical study of single impinging jets through a crossflow. *AIAA Journal of Aircraft* 1989; **26**:1002–1008.
15. Pandya SA, Murman SM, Sankaran V. Unsteady computations of a jet in crossflow with ground effect. *AIAA Paper No. 2003-3898*.
16. Ince NZ, Leschziner MA. Computation of three-dimensional jets in crossflow with and without impingement using second-moment closure. *Engineering Turbulence Modelling and Experiments*. Elsevier Science Publishing Co. Inc.: New York, 1990; 143–153.
17. Tang G, Yang Z, Page GJ, McGuirk JJ. Simulation of an impinging jet in crossflow using an LES method. *Biennial International Powered Lift Conference and Exhibit*, 5–7 November 2002, Williamsburg, Virginia, *AIAA Paper 2002-5959*, 1–8.
18. Daly BJ, Harlow FH. Transport equations in turbulence. *Physics of Fluids* 1970; **13**:2634–2649.
19. Lien FS, Leschziner MA. Assessment of turbulent transport models including non-linear RNG eddy-viscosity formulation and second-moment closure. *Computers and Fluids* 1994; **23**:983–1004.
20. Gibson MM, Launder BE. Ground effects on pressure fluctuations in the atmospheric boundary layer. *Journal of Fluid Mechanics* 1978; **86**:491–511.
21. *Fluent CFD Software 6.1.* Fluent Inc., 10 Cavendish Court, Lebanon, U.S.A.
22. Launder BE, Spalding DB. The numerical computation of turbulent flows. *Computer Methods in Applied Mechanics and Engineering* 1974; **3**:269–289.
23. Launder BE. Shima N. Second-moment closure for the near-wall sublayer: development and application. *AIAA Journal* 1989; **10**:1319–1325.
24. Speziale CG, Sarkar S, Gatski TB. Modelling the pressure–strain correlation of turbulence: an invariant dynamical systems approach. *Journal of Fluid Mechanics* 1991; **227**:245–272.
25. Basara B, Hanjalic K, Jakirlic S, Leschziner MA. Numerical simulation of turbulent flow in a car compartment with a second-moment turbulence closure. *EProc. ASME Fluid Engineering Division Summer Meeting*, *FEDSM97-3023*, 1997.

